Proceedings of the Combustion Institute 40 (2024) 105652

Contents lists available at ScienceDirect

Proceedings of the Combustion Institute

journal homepage: www.elsevier.com/locate/proci

Deepening the knowledge of carbon particulate matter features in the BSS flame configuration

C. Russo [a,*], A. Ciajolo [a], M.M. Oliano [a], B. Apicella [a], M. Sirignano [b]

[a] Istituto di Scienze e Tecnologie per l'Energia e la Mobilità Sostenibili, CNR, P.le V. Tecchio, 80, 80125 Napoli, Italy
[b] Univ. Napoli Federico II, Dipartimento di Ingegneria Chimica, dei Materiali e della Produzione Industriale, Napoli, Italy

ARTICLE INFO

Keywords:
Premixed flame
Particulate matter
Aliphatic hydrogen
Burner-stabilized stagnation flame

ABSTRACT

The paper reports a detailed study on carbon particulate matter (PM) sampled in ethylene flames stabilized on a burner-stabilized stagnation (BSS) system, aiming to give more insights on the characteristics of particles produced in this peculiar flame configuration. The study employs various diagnostic tools to analyze PM collected on the stagnation plate of flames at a constant equivalence ratio (Φ =2.07) and different flame temperatures obtained by varying the cold gas flow velocity. The carbon network of PM was analyzed by Raman and UV–Visible spectroscopy verifying the strong temperature effect on the nanostructure. The FTIR analysis allowed to quantitatively follow the temperature effect on the aromatic and aliphatic C—H bonds, also evaluating the H/C atomic ratio that was found to be rather high (ranging from 0.3 to 0.5) initially decreasing and finally re-increasing as the flame temperature rises. The initial hydrogen loss with the rise of temperature was due to the loss of aromatic hydrogen, followed at higher temperature by the relevant enrichment of hydrogen bonded to aliphatic carbon. This observation is in contradiction with the expectation that higher flame temperatures would lead to an enhanced dehydrogenation of carbon particles, thereby reducing also aliphatic hydrogen. It was suggested that the enrichment in aliphatic hydrogen could be due to the small size of particles having higher radical character and surface area. Indeed, the peculiar features of such carbon particles deserve further work for understanding soot formation and growth and the relevance of BSS carbon material for optical and electronic applications.

1. Introduction

Carbon particulate matter (PM) encompasses the various pollutants produced in the condensed phase from fuel-rich combustion. These include a wide range of components with high molecular weight (MW) and size, extending from polycyclic aromatic hydrocarbons (PAHs) to solid particles and aggregates such as soot [1-3]. Monitoring and controlling carbon PM is essential, due to its significant impact on air quality, human health, and climate change, making it a serious environmental hazard [4,5]. Burner-stabilized stagnation (BSS) flame approach has been proposed by Wang and coworkers [6] as an experimental setup useful for studying soot formation. This experimental configuration guarantees a defined boundary condition downstream of the flame for a more accurate description and control of the perturbation of the flame due to the sampling system. Specifically, the sampling probe is embedded in a water-cooled circular plate positioned above the flame, which acts as flow stagnation surface. This sampling procedure is still intrusive, but the perturbation becomes a boundary condition of the flames, easy to be modeled. Since its introduction, experimental work on BSS configuration has mostly regarded the measure and modeling of particle size distribution (PSD) [7-9], and only few works were devoted to analyze features other than the size of the particles produced in this flame configuration. Wang et al. [9] imaged soot particles by transmission electron microscopy (TEM) evaluating the effective density and measured their carbon to hydrogen atomic ratio, finding a larger C/H ratio in the lower temperature flames. Later, Zhou et al. [10] investigated the size-dependent maturity of soot particles in BSS flame analyzing their nanostructure and oxidation behavior. A similar configuration has been used to investigate the effect of flame temperature in very high temperature conditions (>2100 K) on soot structure by Raman spectroscopy [11]. The peculiarity of BSS configuration relies in the dual nature of the flame. Particles are in fact formed at high temperatures similar to other premixed flame configurations. However, before being collected on the surface of the stabilization plate, particles pass through a zone characterized by a rapid decrease of temperature down to 500 K. The impact of this zone at lower temperature on the PSD

* Corresponding author.
E-mail address: carmela.russo@stems.cnr.it (C. Russo).

https://doi.org/10.1016/j.proci.2024.105652
Received 4 December 2023; Accepted 10 July 2024
Available online 1 August 2024

has been investigated in terms of modeling and it can be substantially linked with an increased coagulation process. However, the role of this zone on the final chemico-physical features of particles lacks a systematic investigation. This is a crucial aspect for different reasons: in combustion research it is important to understand the effect of such cold zones typical of real combustion devices; in the material science field particles with unique features need to be produced in specific conditions.

To fill the gap of knowledge on BSS particles structure and composition, the present work reports about the chemical and spectroscopic characteristics of PM collected on the stagnation plate placed at 12.5 mm of a BSS burner in four ethylene flames previously analyzed as regards temperature, and composition and size of particles collected by a tubular probe [12,13]. The detailed examination of carbon PM features aims:

i) to give more details on the characteristics of soot particles produced in this peculiar flame configuration in the perspective of their relevance in environmental and material science; and
ii) to infer the source of the aliphatic moieties that have been often found to feature soot [13-15] and related to soot dehydrogenation and carbonization [15].

As regards the BSS particle relevance, it is also remarkable that the PM sampled on the cooled stagnation plate of the BSS system (500 K) can be considered representative of PM deposited on "cold-walls" that is an important component of PM emission from engines and turbines.

2. Experimental setup

2.1. Flame reactor and configurations

The experimental campaign concerned sampling and analysis of the composition and nanostructure of PM sampled on the stagnation plate placed at the same height (Hp=12.5 mm) of a benchmark BSS burner. Four ethylene-argon-oxygen flames (C_2H_4: 16.3%, O_2: 23.7%, Ar: 60%) were analyzed fixing the equivalence ratio, Φ=2.07, and changing the maximum temperature [6,12] by changing cold gas velocities, v_0. The investigated flames belong to the C_1–C_6 series that was investigated firstly with the horizontal probe [12], and then in the BSS configuration [6]. The work was focused on the C_3–C_6 series in BSS configuration, so that, by analogy, the flames have been hereafter named BSS-C3 (v_0=8 cm/s), BSS-C4 (v_0=6.53 cm/s), BSS-C5 (v_0=5.50 cm/s), and BSS-C6 (v_0=4.50 cm/s). Flame maximum temperature was measured using an R-type thermocouple. Corrections were applied to account for radiation losses, and gas temperature was derived via an energy balance that considered convective heating and radiative cooling of the bead, while neglecting conduction through the thermocouple wires. The bead's emissivity was assumed to match that of the clean metal, and gas transport properties were estimated as the molar average of the primary gas phase components. Measurements determined flame maximum temperature with uncertainties of ±50 K [16]. The maximum temperatures of the flames were 1885 K for BSS-C3, 1835 K for BSS-C4, 1765 K for BSS-C5 and 1690 K for BSS-C6. The flame was light on whilst a metal cover was positioned onto the stagnation plate to prevent particle deposition during the initial transient regime of the flames. After removing the cover, the carbon PM deposited onto the plate driven by thermophoretic force. A total deposition time of 300 s was used. The temperature at the plate was enough low (around 500 K) to rule out the possibility of sample annealing during the deposition. Particles were mechanically removed from a central spot (2.5 × 2.5 cm^2) of the stabilization plate. The procedure was repeated several times in order to obtain enough material to perform the analysis. For each flame condition sampling was repeated twice.

2.2. Sample treatment and characterization

Raman spectra of PM samples were measured on a Horiba XploRA Raman microscope system (Horiba Jobin Yvon, Japan) using an excitation wavelength of λ = 532 nm (frequency doubled Nd:YAG-solid state laser, 25 mW). FTIR spectra in the 3400–600 cm^{-1} range were acquired on a Nicolet iS10 spectrophotometer, in the transmittance mode, using dispersions prepared by mixing and grinding the carbon PM samples in KBr pellets (0.2–0.3 wt%) [17]. An Agilent UV–Vis 8453 spectrophotometer and a 1-cm path length quartz cuvette were used for measuring UV–Visible (UV–Vis) absorption spectra of the carbon PM suspended in N-methyl-2-pyrrolidinone (NMP) (10 mg/l) and of the <20 nm fraction obtained by filtration of PM suspensions of known concentration (100 mg/l) on an Anotop filter (Whatman, 20 nm of porosity). Carbon PM was suspended, and then analyzed in NMP (100 mg/l) by size exclusion chromatography (SEC) at ambient temperature on a high liquid chromatograph (HPLC) system (HP1050 series), using a Jordi Gel DVB Solid Bead column 300 × 7.8 mm. A HP1050 UV–Vis diode array detector was used as detector of species separated by the SEC column. The uncertainty of the measurements is less than 10%.

3. Results and discussion

Before describing the structural and chemical properties of carbon PM sampled in the BSS flames, it is necessary to remark that, differently from the other flames, the PM formed in the hottest flame (BSS-C3) could not be completely dispersed in NMP. This hindered to apply to it the SEC analysis and the UV–Vis spectroscopy. For this reason, the result section has been divided in two parts: the 3.1 section includes SEC and UV–Vis analysis of PM suspended in NMP limited to PM collected in BSS-C4, BSS-C5 and BSS-C6 flames with a maximum temperature ranging in the 1835–1690 K interval; the 3.2 section is focused on results obtained on powders by Raman and FTIR spectroscopy and includes also the BSS-C3, characterized by the highest maximum temperature flame of 1885 K.

3.1. PM suspension analysis: SEC and UV–Vis analysis of BSS-C4 to BSS-C6 PM

Carbon PM produced in combustion typically comprises varying proportions of a solid component, primarily soot, which significantly contributes to visible absorption. Additionally, it contains an organic carbon fraction that has negligible absorption in the visible spectrum and is soluble in solvents such as dichloromethane and NMP. In order to evaluate the aggregates, the single particles and the organic component distribution of the PM collected in the three flames, SEC analysis has been performed on PM samples suspended in NMP (100 mg/l), recording the absorbance at 350 nm, where both soot and organic components can be detected. For "reading" the SEC profiles in terms of size/MW distribution, it is worth to note that SEC elution typically proceeds with decreasing MW/size as the elution time increases [18]. By calibration with differently sized polystyrene and carbon standards, the first peak (4.5–5 min) is ascribed to particle aggregates (about 100 nm), the second peak (5–5.5 min) is due to single particles (10–20 nm), whereas organic carbon molecules are responsible for the third peak (6 min). Fig. 1 clearly shows that moving from BSS-C4 to BSS-C6 flames, i.e., with the maximum flame temperature decrease, the intensity of the peak relative to aggregates significantly decreases, demonstrating their lower formation in lower temperature conditions. This is consistent with the PSDs measured in similar flame conditions [6,9]. From this analysis the effect of the BSS configuration on particle characteristics appears to be minimal.

The UV–Vis spectra are influenced by both the relative contribution and specific absorption characteristics of the organic carbon and soot components. Therefore, the trends in the UV–Vis mass absorption coefficients (MAC) of BSS-C4, BSS-C5, and BSS-C6 PM, reported in Fig. 2, should be interpreted considering the variation in both the relative

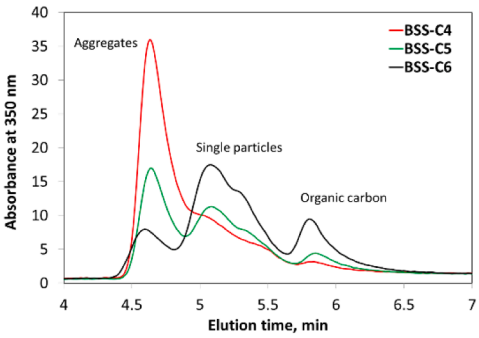

Fig. 1. SEC profiles of NMP-dispersed PM (100 mg/l) sampled in BSS-C4, BSS-C5 and BSS-C6 flames.

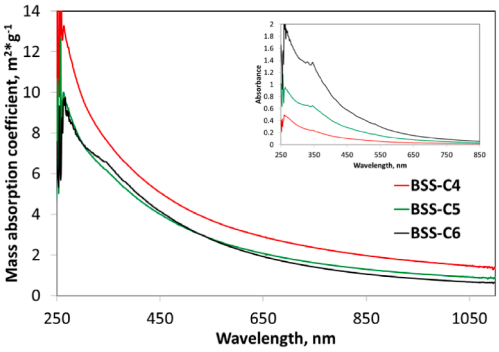

Fig. 2. UV–Vis mass absorption coefficient of BSS-C4, BSS-C5 and BSS-C6 PM samples. Inset: UV–Vis spectra of the <20 nm PM fraction obtained from PM suspensions of 100 mg/l.

proportions and specific MAC of soot and organic carbon as a function of the flame temperature [15,19]. It can be noticed that the MAC of PM at 500 nm is around 4 m^2/g, next to the values measured for soot in premixed flames [15,19], and not far from the values measured for carbon aerosol [5]. Provided that soot is the main contributor to the PM absorption in the visible, the significant increase in the visible of the PM absorption from BSS-C6 and BSS-C5 to the BSS-C4 flame can be mainly associated to the increase of soot contribution to the total PM. This is corroborated by the diminished intensity of single particle and organic carbon peaks of BSS-C4 (Fig. 1). This finding is consistent with the general assessment that, at fixed equivalence ratio, in comparison to organic species, soot formation increases with flame temperature increase [20,21]. Hence, once again, the impact of the BSS configuration on PM features appears negligible.

It has to be remarked that the organic carbon contribution (last peak in Fig. 1) is generally low in comparison to those of single particles and aggregates. This is consistent with the very low contribution of UV–Vis spectra of organic carbon to the PM spectra found in all flames. The temperature effect on the PM absorption is not as well clear passing from BSS-C5 to BSS-C6 flames presenting similar absorption in the UV–Vis range. However, the slightly higher and more structured absorption in the UV of the BSS-C6 PM can be observed in comparison to BSS-C5 PM and ascribable to the increase of organic species contribution (last peak of Fig. 1), mainly absorbing in the UV region. Consistently, the UV–Vis spectrum of the BSS-C6 organic carbon, i.e., the <20 nm fraction obtained by filtration of PM suspensions of 100 mg/l (inset of Fig. 2), shows the higher absorbance values and the finer spectral structure in comparison to BSS-C4 and BSS-C5 organic carbon.

UV–Vis spectroscopy provides not only information on the composition and absorbance strength of carbon PM, but also on its nanostructure. Indeed, the use of the dispersion exponent and optical band gap derived from absorption spectra, firstly proposed by Millikan [23], D'Alessio et al. [24], and Minutolo et al. [25], has been extensively utilized to probe soot maturity and nanostructure. The comparison of the UV–Vis spectra of BSS-C4, BSS-C5 and BSS-C6 PM samples, reported as a function of the photon energy in the supplemental material (Fig. S1), clearly shows how the broad band edge shifts toward higher energies, i.e., toward lower wavelengths, going from the hottest (BSS-C4) to the coolest (BSS-C6) flame. This shift is better shown in the inset of Fig. S1 reporting the absorbance in the Tauc domain. In this study, we have applied a recently refined optical band gap method [22,26] for discriminating and evaluating the optical properties and contributions of organic carbon and soot directly from the PM absorption spectra. The method allows evaluating the dispersion exponent, α, of soot and the optical band gap of both PM components, reported in Table 1 along with other optical parameters below discussed. Low α values, 1.3–1.4, of BSS-C4 PM and soot fraction are closer to the values typically found for black carbon and mature soot [22,27,28]. Relatively higher values of α, around 2, are observed for the lowest temperature conditions of the BSS-C6 PM and soot fraction, approaching those of newly-formed particles [28]. It is noteworthy that the BSS-C6 fraction with size smaller than 20 nm significantly absorbs in the visible region and is characterized by a slightly lower band gap (see inset of Fig. 2 and Table 1). A low bang gap value for the BSS-C4 soot fraction was found as typically evaluated for mature soot [22]. Relatively higher values of band gap are observed for the lowest temperature condition, more typical of soot formed in the transition from young to mature soot of premixed flames [22]. Overall, both the dispersion exponent and optical band gap of soot decrease with the increase of flame temperature, whereas negligible changes of organic carbon optical parameters occur going from BSS-C6 to BSS-C4 (Table 1). The relevant variation of the optical parameters of soot demonstrates significant soot structural changes for effect of maximum flame temperature. The optical band gap can unveil the structural properties of aromatic absorbers in disordered carbons as it can be used to estimate the aromatic size, L_a, of the basic structural unit featuring carbon nanostructure [22,29]. The band gap decrease corresponds to an increase of aromatic system size featuring hydrogenated amorphous carbons [29]. The optical band gap values for organic carbon hint to a low size of aromatic unit (less than 15 rings) [22]. As regards soot, the optical band gap decrease is just a signature of the increase of carbon clustering into aromatic domains. In fact, the proposed empirical relation between L_a and optical band gap fails to quantitatively describe the internal structure of sp^2-rich (hydrogen-poor) materials as mature soot [26].

Overall, the particle size distribution and spectral analysis described above highlight the progressive decrease of organic carbon contribution and the enhancement of soot carbonization with the flame temperature increase, at least up to 1835 K, in agreement with previous works on premixed flames [19-21]. This demonstrates that the BSS configuration does not impact on particle features so far discussed. Unfortunately, as above mentioned, this analysis could not be extended to the BSS-C3 flame because it was not possible to get stable dispersions of the BSS-C3 PM sample in NMP. The reason of this peculiarity have been investigated by further analysis on BSS-C3 PM and the other PM samples

Table 1
Optical parameters of carbon PM and related fractions. Soot and organic carbon values were derived from the method reported in [22].

	PM exp disp	Soot exp disp	Soot Eg, eV	Organic Carbon Eg, eV	PM I(D)/I (G)
BSS-C3	n.d.	n.d.	n.d.	n.d.	0.95
BSS-C4	1.47	1.31	0.25	1.64	0.88
BSS-C5	1.74	1.51	0.37	1.6	0.76
BSS-C6	2.15	1.85	0.54	1.57	0.77

in powder form.

3.2. PM powder analysis: RAMAN and FTIR spectroscopy of BSS-C3 to BSS-C6 PM

The Raman spectra of PM collected in all the flames, reported in Fig. 3, exhibit the two typical peaks of carbon materials, near 1600 cm^{-1} (G peak), assigned to the C = C stretching of all pairs of sp^2 atoms, and at 1350 cm^{-1} (D peak) due to the breathing modes of sp^2 atoms in rings [30]. Beside the D and G bands, other minor modulations, induced by defects outside and inside the crystal lattice, occur next to the G peak and in the 1100–1300 cm^{-1} region. An accurate Raman spectral analysis and deconvolution procedure has been set up in a previous work on soot [31] and used in this work making allowance of the contributions and features of the main and minor peaks. The deconvoluted spectra are reported in Fig. S2 of the supplemental material. Tuinstra and Koenig demonstrated that the D mode intensity increases with decreasing graphite crystal size until 2 nm: below this size this trend does not hold due to increased defects [30].

This implies that, in disordered carbons like soot, the development of the D peak indicates ordering, exactly opposite to the case of graphite [30]. Consequently, the increase of the D to the G peak intensity ratio, I (D)/I(G), going from BSS-C6 to BSS-C3, (Table 1), confirms the occurrence of the progressive ordering and/or aromatization growth with flame temperature of the carbon nanostructure, above observed by SEC and UV–Vis analysis of PM suspensions. In this regard, Raman analysis is consistent with the hypothesis that the main structure of particle is formed in the early stages of the flames where the temperature reaches the maximum value.

Further details on the compositional changes occurring with temperature increase have been investigated by FTIR spectroscopy offering some intriguing clues to the features of BSS PM. The MAC values of PM in the 3200–500 cm^{-1} wavenumber range, reported in Fig. 4, show some peaks emerging from the absorption background, the latter one being mainly due to the carbon network. The FTIR absorption trend is consistent with that measured in the UV–Vis range, being BSS-C6 and BSS-C5 samples the less light-absorbing PM in comparison to BSS-C4 (Fig. 2). This confirms the enhancement of carbonization process as flame temperature rises.

To put in evidence some peaks related to carbon functionalities [15,17], the C—H stretching region was continuum subtracted with a linear correction between 4000 and 2500 cm^{-1} wavenumber region. The same procedure was adopted in the region between 2000 and 600 cm^{-1}. In Fig. 5 the FTIR spectra in the 2700–3200 cm^{-1} (normalized on the intensity of the peak at 2925 cm^{-1}, top panel) and in the 600–2000 cm^{-1} wavenumber range (normalized on the intensity of the peak at 1600 cm^{-1}, lower panel) are reported deprived of the continuum background.

In the 3000–2800 cm^{-1} wavenumber range (top panel of Fig. 5), it can be seen that peaks due to the stretching of aliphatic C—H bonding, associated to what here is briefly named aliphatic hydrogen, are present mainly in form of methylene groups responsible of the most intense peak

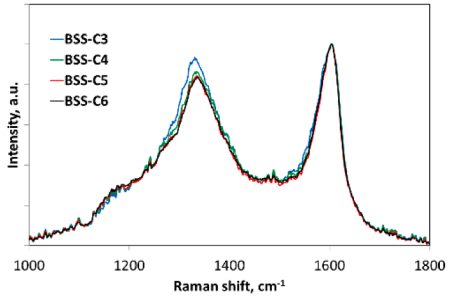

Fig. 3. Raman spectra (normalized on the 1600 cm^{-1} peak) of BSS-C3, BSS-C4, BSS-C5 and BSS-C6 PM samples.

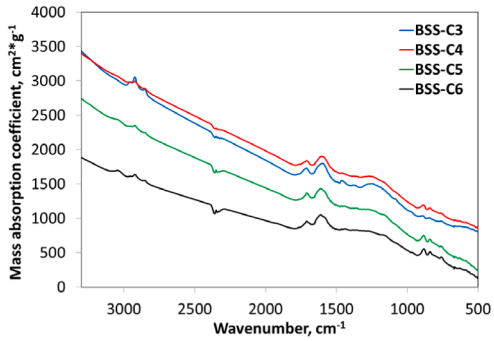

Fig. 4. FTIR spectra of BSS-C3, BSS-C4, BSS-C5 and BSS-C6 PM samples.

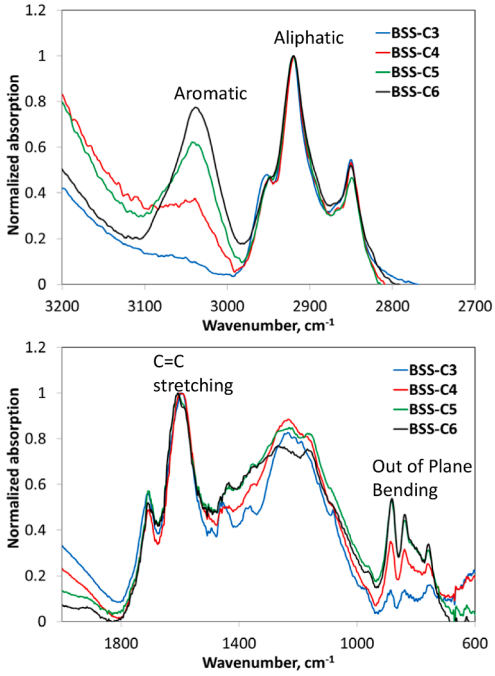

Fig. 5. Normalized FT-IR spectra in the 3200–2750 cm^{-1} (top panel) and 2000–600 cm^{-1} (low panel) region of BSS-C3, BSS-C4, BSS-C5 and BSS-C6 PM samples.

at 2925 cm^{-1}. In comparison to the aliphatic C—H signals, the aromatic C—H stretching signal, at about 3050 cm^{-1}, decreases with flame temperature and even disappears for the BSS-C4 and BSS-C3 flames. The aromatic C—H functionalities, associated to what here is briefly named aromatic hydrogen, can be more easily detected in the 900–700 cm^{-1} range (bottom panel of Fig. 5), where the out-of-plane (OPLA) C—H bending of aromatic systems occurs. In comparison to the 1600 cm^{-1} peak, due to C = C bond stretching, the loss of aromatic hydrogen with temperature is noticeable. Also, the narrowing and increasing intensity with the flame temperature of the broad peak around 1200 cm^{-1} can be observed, possibly due to the increasing presence of odd-carbon number rings, as found for fullerenic soot [17], so corresponding to the increase of bending/curvature of graphene layers featuring small particles.

The spectrum in the 2700–3200 cm^{-1} stretching region was deconvoluted into its main components, taking into account also for the contribution of the broad OH stretching peak at about 3600 cm^{-1}. Applying a quantitative method developed in a previous work [17], the aliphatic and aromatic hydrogen percentages along with the H/C atomic ratios of the PM samples have been estimated and are displayed in Fig. 6. While the occurrence of “aromatic carbon dehydrogenation” with the increase in flame temperature is expected, the corresponding aliphatic

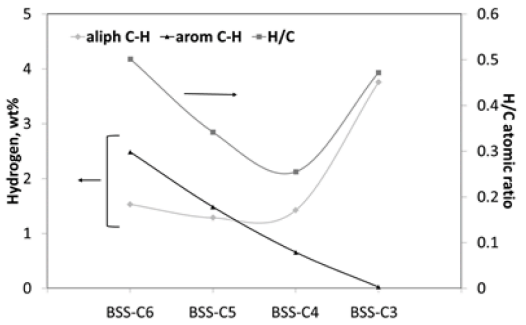

Fig. 6. Aliphatic and aromatic hydrogen content, and H/C atomic ratio of BSS-C3, BSS-C4, BSS-C5 and BSS-C6 PM samples.

hydrogen enrichment is remarkable. The partial capability of NMP to disperse BSS-C3 PM, which appears as a supernatant, is in agreement with the peculiar characteristics of this sample, namely the abundance of aliphatic functionalities. In fact, NMP, highly efficient in achieving stable carbon solid dispersions, even useful for exfoliating graphene layers from bulk graphite [32], fails to disperse carbon-based materials in which the presence of aliphatic carbon is significant [33]. Unexpectedly, BSS-C3 PM appears very much hydrogenated, similarly to the BSS-C6 PM (approaching hydrogen-to-carbon atomic ratio (H/C = 0.5), but it is completely devoid of aromatic hydrogen. Interestingly, the average H/C atomic ratio of the BSS samples analyzed in the present work is high (0.3–0.5) consistently with previous work [9] where the aliphatic hydrogen character was only presumed. Typically, soot characterized by a high hydrogen-to-carbon ratio, significantly greater than 0.1, exhibits elevated ratios of aromatic to aliphatic hydrogen and is usually present at the inception and in the cooler flames of aliphatic hydrocarbons [15]. Thus, on our knowledge, a PM with the features of the BSS-C3 sample, i.e., a high aromatic character and at the same time a high abundance of aliphatic hydrogen, has never been observed before.

The aliphatic hydrogen enrichment, namely a higher aliphatic C—H/aromatic C—H ratio, has been found for the first time on soot particles sampled by a tubular probe in premixed flames burning in similar conditions [13]. By contrast in fuel richer (Φ =2.4) premixed ethylene and methane flames [15], it has been found that, as dehydrogenation occurs, aromatic hydrogen remains always more abundant than aliphatic hydrogen both persisting downstream the flames, especially in the methane flame.

Interestingly, a similar aliphatic enrichment has been observed just for organic carbon in ethylene [20,34] and benzene flames [21,35]. In these cases, organic carbon was initially found to be characterized by a high concentration of aromatic hydrogen, attributed to PAHs, and then, downstream in the flame, it became increasingly enriched in aliphatic hydrogen. It is important to underscore that the possibility that the aliphatic contribution could be due to condensed matter sticked at relatively low temperature onto particle surface can be excluded since it should have been removed by NMP dispersion and ultrasonic bath treatment, so allowing PM stable dispersion. These observations imply that aliphatic functional groups are chemically attached to the particles. The high temperature and unique configuration of the BSS, somehow favoring surface reactions, could be at the basis of these findings. However, in light of the data reported in this work the low temperature zone of the flame is a necessary condition, but certainly not sufficient, to the formation of aliphatic components on soot, as depicted by Wang under specific conditions [13]. Indeed, the temperature variation among the four conditions appears not markedly significant and all the PM particles experienced the low temperature region. It has to be also considered that surface reaction should be much more favoured for BSS-C5 and BSS-C6 flames because their lower cold gas velocities correspond to longer residence times. Looking at the relative contribution of aliphatic and aromatic C–H [13] it has been found that the aromatic/aliphatic ratio is low (<0.2) early in the flame and almost constant already at 10 mm of Hp. To reconcile these considerations on temperature profile and residence time with peculiar features of PM, a pivotal examination of particle size is warranted, particularly to particle specific surface area. Wang et al. [9] measured by TEM the diameter of primary particles in the BSS configuration in similar flame conditions reporting a strong diameter reduction as the maximum temperature of the flame increases with a significant reduction of soot volume fraction. Similar trends have been reported for flames with the same feed, but not in the BSS configuration [13]. The higher specific surface area of BSS-C3 soot particles can accommodate, relatively faster, aliphatic functionalities onto the surface. As the particle diameter decreases, the arising of layer distortions with warping and puckering phenomena occurs leading to bending/curvature of graphene structures characterized by a mixed sp^2–sp^3 hybridization state, symptomatic of a higher reactivity of C—H bonds [36]. Beside the small sizes, it can be speculated that PM has a very high radical character favouring the surface reaction with environment gases. Overall, the combination of the investigated conditions and burner configurations favored the production of unique particles. The equilibrium for producing these particles is very delicate and yet to be completely understood. Also, the peculiarities of the particles produced in C3 flames, shown by the detailed analysis here reported, require further work as presenting intriguing avenues for future investigations into their optoelectronic and physicochemical properties.

4. Conclusions

This paper presents an in-depth analysis of the properties of carbon PM collected from ethylene flames produced at a fixed equivalence ratio (Φ =2.07) in the BSS configuration. For the first time, Raman, UV–Vis and FTIR spectroscopy, and size exclusion chromatography were employed for the PM analysis in BSS flames. The aim was to deepen the knowledge of the features of the particles produced in this configuration, widely used in combustion research, focusing the attention on assessing how maximum flame temperatures and the low temperature zone influence soot characteristics in this particular flame setup.

Overall, the paper highlights that the nanostructure of the BSS-C4-C6 particles was significantly influenced by the increasing temperatures in the high-temperature zone, causing higher clustering and aromatization of carbon network as temperature rises. This is a trivial result accompanied by a not trivial and unexpected result for the highest temperature flame, BSS-C3, that is a strong hydrogenation mainly pertinent to aliphatic hydrogen. Specifically, for the highest temperature condition, carbon particles have been detected having unique and unprecedented characteristics, i.e., highly carbonized aromatic nanostructure and high content of hydrogen. Differently from particles generally found in other fuel-richer flame conditions, these particles, were scarcely dispersible in NMP consistently with the shortage of aromatic hydrogen and higher aliphatic hydrogen content, mainly present in form of aliphatic CH_2 groups linked on the aromatic carbon network as found by quantitative FTIR spectroscopy. Overall, the H/C atomic ratio was found to initially decrease and re-increase as the maximum flame temperature rises. The initial dehydrogenation, due mainly to the loss of aromatic hydrogen, is followed by the enrichment of hydrogen bonded to aliphatic carbon. This observation is in contradiction to the expectation that higher flame temperatures would lead to greater dehydrogenation and carbonization of soot, thereby reducing the presence of surface-attached aliphatic groups. It can be speculated that, in spite of the shorter residence times, surface reactions are favoured on the smaller particles featuring the highest temperature BSS flame, having a high specific surface area, curved layers, and presumably higher radical character.

Novelty and significance statement

This work provides an in-depth understanding of the characteristics of carbon particulate matter from ethylene flames in a burner-stabilized

stagnation configuration, a flame set-up widely diffused in combustion research. The study revealed that carbon particles can exhibit unique characteristics depending on the flame temperature. Notably, particles formed at higher temperatures exhibited strong hydrogenation, predominantly in the form of aliphatic groups attached to the aromatic carbon network. This is a non-trivial and unexpected result contradicting the expectation that higher flame temperatures would lead to greater dehydrogenation of soot, thus reducing the presence of surface-attached functional groups. The paper highlights how surface reactions are favored on small particles, characterized by a large specific surface area and curved layers, and a high radical character. These findings offer new insights into the flame-synthesis of carbon nanoparticles with peculiar properties and challenge current understandings of the soot particle formation process under high-temperature conditions.

Author contributions

- Carmela Russo, Data analysis, conceptualization, writing original draft, supervision, funding acquisition
- Anna Ciajolo Data analysis, conceptualization, writing original draft, supervision
- Maria Maddalena Oliano Data collection and analysis, writing original draft
- Barbara Apicella Data analysis, conceptualization, writing original draft, supervision
- Mariano Sirignano Data analysis, conceptualization, writing original draft, supervision, funding acquisition

Declaration of competing interest

The authors declare that they have no known competing financial interests or personal relationships that could have appeared to influence the work reported in this paper.

Acknowledgements

The authors acknowledge funding from PRIN project STANDALONE, Code: 2022L5K3MB, “Fondo per il Programma Nazionale della Ricerca (PNR) e Progetti di Ricerca di Rilevante Interesse Nazionale (PRIN)” - Finanziato dall’Unione europea – NextGenerationEU under PIANO NAZIONALE DI RIPRESA E RESILIENZA (PNRR)Missione 4 - Componente 2 - Investimento 1.1. The authors thank Prof. Hai Wang to kindly provide the BSS burner.

Supplementary materials

Supplementary material associated with this article can be found, in the online version, at doi:10.1016/j.proci.2024.105652.

References

[1] H. Bockhorn, A D’Anna, A.F. Sarofim, H. Wang (Eds.), Combustion Generated Fine Carbonaceous Particles, Karlsruhe University Press, Karlsruhe, Germany, 2009.
[2] B.S. Haynes, H.G. Wagner, Soot formation, Prog. Energy Combust. Sci. 7 (1981) 229–273.
[3] H. Wang, Formation of nascent soot and other condensed-phase materials in flames, Proc. Combust. Inst. 33 (2011) 41–67.
[4] S.Y. Kyung, S.H. Jeong, Particulate-matter related respiratory diseases, Tuberc. Respir. Dis. 83 (2020) 116–121.
[5] T.C. Bond, R.W. Bergstrom, Light absorption by carbonaceous particles: an investigative review, Aerosol. Sci. Technol. 40 (2006) 27–67.
[6] A.D. Abid, J. Camacho, D.A. Sheen, H. Wang, Quantitative measurement of soot particle size distribution in premixed flames - the burner-stabilized stagnation flame approach, Combust. Flame 156 (2009) 1862–1870.
[7] J. Camacho, C. Liu, C. Gu, H. Lin, Z. Huang, Q. Tang, et al., Mobility size and mass of nascent soot particles in a benchmark premixed ethylene flame, Combust. Flame 162 (2015) 3810–3822.
[8] H. Lin, C. Gu, J. Camacho, B. Lin, C. Shao, C. Li, et al., Mobility size distributions of soot in premixed propene flames, Combust. Flame 172 (2016) 365–373.
[9] M. Wang, Q. Tang, J. Mei, X. You, On the effective density of soot particles in premixed ethylene flames, Combust. Flame 198 (2018) 428–435.
[10] Y. Zhou, M. Wang, Q. He, X. You, Experimental investigation on the size-dependent maturity of soot particles in laminar premixed ethylene burner-stabilized stagnation flames, Proc. Combust. Inst. 39 (2023) 1147–1155.
[11] J. Bonpua, Y. Yagües, A. Aleshin, S. Dasappa, J. Camacho, Flame temperature effect on sp2 bonds on nascent carbon nanoparticles formed in premixed flames (Tf, max >2100 K): A Raman spectroscopy and particle mobility sizing study, Proc. Combust. Inst. 37 (2019) 943–951.
[12] A.D. Abid, N. Heinz, E.D. Tolmachoff, D.J. Phares, C.S. Campbell, H. Wang, On evolution of particle size distribution functions of incipient soot in premixed ethylene-oxygen-argon flames, Combust. Flame 154 (2008) 775–788.
[13] J.P. Cain, P.L. Gassman, H. Wang, Laskin A, Micro-FTIR study of soot chemical composition - evidence of aliphatic hydrocarbons on nascent soot surfaces, PCCP 12 (2010) 5206–5218.
[14] M.S. Akhter, A.R. Chughtai, D.M. Smith, The structure of hexane soot I: spectroscopic studies, Appl. Spectrosc. 39 (1985) 143–153.
[15] C. Russo, A. Tregrossi, A. Ciajolo, Dehydrogenation and growth of soot in premixed flames, Proc. Combust. Inst. 35 (2015) 1803–1809.
[16] C. Russo, A. D’Anna, A. Ciajolo, M. Sirignano, The effect of butanol isomers on the formation of carbon particulate matter in fuel-rich premixed ethylene flames, Comb. Flame 199 (2019) 122–130.
[17] C. Russo, F. Stanzione, A. Tregrossi, A. Ciajolo, Infrared spectroscopy of some carbon-based materials relevant in combustion: qualitative and quantitative analysis of hydrogen, Carbon 74 (2014) 127–138.
[18] M. Alfè, B. Apicella, R. Barbella, A. Tregrossi, A. Ciajolo, Distribution of soot molecular weight/size along premixed flames as inferred by size exclusion chromatography, Energy Fuel. 21 (2007) 136–140.
[19] C. Russo, M. Alfè, J.-N. Rouzaud, F. Stanzione, A. Tregrossi, A. Ciajolo, Probing structures of soot formed in premixed flames of methane, ethylene and benzene, Proc. Combust. Inst. 34 (2013) 1885–1892.
[20] A. Ciajolo, A. D’anna, R. Barbella, A. Tregrossi, A. Violi, The effect of temperature on soot inception in premixed ethylene flames, Symp. (Int.) Combust. 26 (1996) 2327–2333.
[21] C. Russo, F. Stanzione, A. Tregrossi, M. Alfè, A. Ciajolo, The effect of temperature on the condensed phases formed in fuel-rich premixed benzene flames, Combust. Flame 159 (2012) 2233–2242.
[22] C. Russo, B. Apicella, A. Tregrossi, A. Ciajolo, K. Cuong Le, S. Török, P.-E. Bengtsson, Optical band gap analysis of soot and organic carbon in premixed ethylene flames: Comparison of in-situ and ex-situ absorption measurements, Carbon 158 (2020) 89–96.
[23] R.C. Millikan, Optical properties of soot, J. Opt. Soc. Am. 51 (1961) 698–699.
[24] A. D’Alessio, F. Beretta, C. Venitozzi, Optical investigations on soot forming methane-oxygen flames, Combust. Sci. Technol. 5 (1972) 263–272.
[25] P. Minutolo, G. Gambi, A. D’Alessio, The optical band gap model in the interpretation of the UV-visible absorption spectra of rich premixed flames, Symp. (Int.) Combust. 26 (1996) 951–957.
[26] C. Russo, B. Apicella, A. Ciajolo, Hydrogen, sp2 carbon hybridization, and sp2 clustering as pieces of the puzzling nanostructure of soot: a closer look, Energy Fuel. 37 (2023) 12525–12540.
[27] H.A. Michelsen, Probing soot formation, chemical and physical evolution, and oxidation: A review of in situ diagnostic techniques and needs, Proc. Combust. Inst. 36 (2017) 717–735.
[28] J. Simonsson, N.E. Olofsson, S. Török, P.E. Bengtsson, H. Bladh, Wavelength dependence of extinction in sooting flat premixed flames in the visible and near-infrared regimes, Appl. Phys. B 119 (2015) 657–667.
[29] J. Robertson, Hard amorphous (diamond-like) carbons, Prog. Solid State Chem. 21 (1991) 199–333.
[30] A.C. Ferrari, J. Robertson, Interpretation of Raman spectra of disordered and amorphous carbon, Phys. Rev. B 61 (2000) 14095–14107.
[31] C. Russo, A. Ciajolo, Effect of the flame environment on soot nanostructure inferred by Raman spectroscopy at different excitation wavelengths, Combust. Flame 162 (2015) 2431–2441.
[32] M. Cai, D. Thorpe, D.H. Adamson, H.C. Schniepp, Methods of graphite exfoliation, J. Mater. Chem. 22 (2012) 24992–25002.
[33] R. Kandiyoti, A. Herod, K.D. Bartle, J.M. Morgan, Solid Fuels and Heavy Hydrocarbon Liquids: Thermal Characterization and Analysis, Elsevier Science, 2017, p. 416.
[34] A. Ciajolo, B. Apicella, R. Barbella, A. Tregrossi, Correlations of the spectroscopic properties with the chemical composition of flame-formed aromatic mixtures, Combust. Sci. Technol. 153 (2000) 19–32.
[35] J.T. McKinnon, E. Meyer, J.B. Howard, Infrared analysis of flame-generated PAH samples, Combust. Flame 105 (1996) 161–166.
[36] J.B. Howard, Carbon addition and oxidation reactions in heterogeneous combustion and soot formation, Sympos. (Int.) Combust. 23 (1991) 1107–1127.